Research Square

Preprints are preliminary reports that have not undergone peer review.
They should not be considered conclusive, used to inform clinical practice,
or referenced by the media as validated information.

Chiral Discrimination and Mechanistic Study of Enantiomers R-1,1'-Bi-2-naphthol and S-1,1'-Bi-2-naphthol in Briggs-Rauscher Oscillatory Chemical System

Lanlan Zhang
Anhui Xinhua University
Ali Tao
Anhui Xinhua University
Ling Zhu
Anhui Xinhua University
Gang Hu
zhanglanlan@axhu.edu.cn

Anhui University

Research Article

Keywords: Chiral discrimination, Enantiomers, R-1,1'-bi-2-naphthol (R-BINOL), S-1,1'-bi-2-naphthol (S-BINOL), Briggs–Rauscher oscillatory system, Inhibition time

Posted Date: August 24th, 2026

DOI: https://doi.org/10.21203/rs.3.rs-10650271/v1

License: This work is licensed under a Creative Commons Attribution 4.0 International License.
Read Full License

Additional Declarations: No competing interests reported.

Chiral Discrimination and Mechanistic Study of Enantiomers R-1,1'-Bi-2-naphthol and S-1,1'-Bi-2-naphthol in Briggs-Rauscher Oscillatory Chemical System

Lanlan Zhang[1,2], Ali Tao[1], Ling Zhu[1], Gang Hu[2,*]
[1] School of Pharmacy, Anhui Xinhua University; Hefei 230088, China;
[2] School of Chemistry Chemical Engineering, Anhui University; Hefei 230601, China
*Corresponding author: Gang Hu, email: zhanglanlan@axhu.edu.cn

Abstract
A novel method for the qualitative discrimination of the axial enantiomers R-1,1′-bi-2-naphthol (R-BINOL) and S-1,1′-bi-2-naphthol (S-BINOL) was developed using the Briggs–Rauscher (B-R) oscillatory system catalyzed by $[NiL](ClO_4)_2$ (L = 5,7,7,12,14,14-hexamethyl-1,4,8,11-tetraazacyclotetradeca-4,11-diene). Addition of either enantiomer at identical concentrations temporarily inhibited the oscillations, yet produced distinctly different inhibition times (t_in). Over the concentration range 1.25×10^{-6} to 6.25×10^{-6} mol/L, R-BINOL consistently gave longer t_in values than S-BINOL (e.g., 255.6 s vs 183.5 s at 1.25×10^{-6} mol/L; 1538.4 s vs 1131.6 s at 6.25×10^{-6} mol/L), enabling clear qualitative discrimination. Cyclic voltammetry indicated that hydroperoxyl radicals (HOO•) participate in the oxidation of the phenolic hydroxyl groups. Infrared spectroscopy confirmed conversion of the hydroxyl groups into carbonyl functionalities. The different inhibitory behaviors are interpreted within the Free Radical Controlled Autoinhibition (FCA) framework, in which R-BINOL more effectively scavenges HOO•, thereby more strongly disrupting the radical balance required for sustained oscillation. The results demonstrate that B-R oscillatory systems can serve as simple, sensitive platforms for chiral discrimination.

Keywords: Chiral discrimination · Enantiomers · R-1,1′-bi-2-naphthol (R-BINOL) · S-1,1′-bi-2-naphthol (S-BINOL) · Briggs–Rauscher oscillatory system · Inhibition time

Introduction

R-1,1'-Bi-2-naphthol (R-BINOL) and S-1,1'-Bi-2-naphthol (S-BINOL), whose structures are shown in Scheme 1, possess distinctive axial chirality and are widely used in organic synthesis. Both enantiomers can serve as effective chiral ligands and form chiral metal catalysts with metals such as palladium and rhodium. These catalysts have been applied in a range of asymmetric transformations, including asymmetric hydrogenation [1], asymmetric carbon–carbon bond formation, and asymmetric oxidation. In the 1980s, Sharpless and co-workers pioneered highly enantioselective syntheses of selected olefinic alcohols using chiral catalysts [2]. R-BINOL and S-BINOL can also be incorporated into chiral phase-transfer catalysts (CPTCs), thereby promoting high enantioselectivity in phase-transfer reactions. In addition, their derivatives may function as chiral auxiliaries that improve product enantioselectivity through steric interactions with substrates. R-BINOL and S-BINOL are valuable starting materials for the preparation of chiral organic compounds [3,4] and therefore

play important roles in the synthesis of pharmaceuticals, fine chemicals, and chiral materials. More broadly, they are frequently employed as foundational building blocks for novel reaction types and synthetic strategies in chiral chemistry. Their rigid, stereochemically defined binaphthyl frameworks also provide useful photophysical properties, supporting applications in organic luminescent materials [5,6]. Consequently, reliable discrimination between R-BINOL and S-BINOL is of substantial analytical and practical significance.

The discrimination of chiral enantiomers remains a challenging problem in analytical chemistry because enantiomeric pairs exhibit nearly identical physical and chemical properties in achiral environments. Several methods have been investigated for differentiating R-BINOL and S-BINOL, yet each has practical limitations. Laser polarimetry [7], for example, has been applied to chiral analysis, although measurement reliability may be affected by operational factors and data-transfer accuracy [8]. Structural methods, including ^{1}H NMR, ^{13}C NMR and the Mosher method [9], have also been used. However, these approaches may require costly chiral derivatization reagents and can be complicated by substantial shielding effects involving the aromatic protons [10–12]. X-ray single-crystal diffraction (XRD) provides direct structural information but depends on the successful preparation of single crystals of suitable size and quality [13–15]. Optical rotatory dispersion (ORD) spectroscopy has also been employed but is limited by low signal intensity, high technical requirements, and low sensitivity for non-aqueous samples [16–18]. Separation-based techniques, such as high-performance capillary electrophoresis (HPCE) with chiral selectors and high-performance liquid chromatography (HPLC) with chiral stationary phases, have likewise been used [19,20]. Although these techniques can provide effective enantiomeric separation, they may require specialized materials and instrumentation; in HPLC, frictional heating within the column may also affect performance under some operating conditions. These limitations motivate the development of simpler, faster, and more cost-effective strategies for enantiomer discrimination.

Differentiating enantiomers through chemically catalyzed kinetics is particularly difficult because the two species generally display highly similar reactivity. To the best of our knowledge, chemical oscillation-based methods have rarely been explored for this purpose. The present study therefore investigates a new strategy for discriminating the optical isomers R-BINOL and S-BINOL using the Briggs–Rauscher (B-R) chemical oscillation system. The approach evaluates the characteristic perturbation produced by each enantiomer in the oscillatory reaction. By relating these perturbations to inhibition time and supporting mechanistic evidence, the method provides a simple, rapid, and cost-effective route for distinguishing the two enantiomers and offers a new perspective on chiral analysis based on nonlinear chemical dynamics.

Instruments and reagents

Reagents

Purchased reagents

Sulfuric acid (98%, Todd Chemical Co. Ltd.), potassium iodate (Henan Juxing Chemical Co. Ltd.), malonic acid (Guangdong Rongjiang Chemical Co. Ltd.), hydrogen peroxide (30%, Xinxiang

Juyuan Technology Co. Ltd.), R-BINOL, S-BINOL (99%, Shanghai Macklin Biochemical Co. Ltd), and the catalyst $[NiL](ClO_4)_2$. Concentrations of prepared solutions are 0.025M sulfuric acid, 2M potassium iodate, 0.02M catalyst $[NiL](ClO_4)_2$, 0.14M malonic acid, and 3.5M hydrogen peroxide. A 0.002M sulfuric acid stock solution was used for preparation.

Laboratory Preparation of Reagents Macrocyclic Nickel Catalysts

The catalyst utilized in this study was synthesized according to the procedure described in reference [21]. The preparation process involved two steps. Firstly, the ligand $L{\cdot}2HClO_4$ was prepared, where L represents 5,7,7,12,14,14-hexamethyl-1,4,8,11- tetraazacyclotetradeca- 4,11-diene. The molecular structure of the ligand is depicted in scheme 2(left). Following this, the catalyst $[NiL](ClO_4)_2$ was synthesized using the ligand $L{\cdot}2HClO_4$, and its structure is illustrated in scheme 2(right). (see scheme 2 in supplementary materials)

In chemical oscillatory reaction systems, macrocyclic nickel complexes can potentially replace Mn^{2+} and Ce^{3+} as catalysts. The present catalyst offers several advantages associated with its macrocyclic coordination geometry: (a) the ligand contains a π-conjugated macrocyclic framework that can facilitate electron transfer and thereby promote rapid reaction kinetics; (b) complexation with metal ions produces favorable oscillation parameters and may lower the energy of key reaction intermediates; and (c) the resulting chemical oscillations are reproducible, decay slowly, and persist for an extended period. An appropriate quantity of the dried catalyst was analyzed by infrared spectroscopy. The spectrum was consistent with the presence of C=N, =C-H, $-CH_3$, C-N, and N-H functional groups in the synthesized tetraazacyclotetradeca-diene nickel complex.

Instruments and operating procedures

Instruments

Electrochemical workstation (CHI6001, Shanghai Chenhua Instruments), infrared spectrophotometer (AIM-9000, Shimadzu, Japan), platinum electrode, saturated calomel electrode, amplifier, go!Link (Vernier, USA), and a micropipette (20µl - 200µl, Shanghai Leici).

Operating procedures

Firstly, initialize the Logger Lite testing application, setting the sampling duration to 3000s with a sampling rate of 0.5s per instance. Following this, prepare a reactant solution in a beaker by incorporating the given substances in the subsequent order: 11ml of 0.025M sulfuric acid, 6.5ml of 2M Potassium iodate, 3.5ml of 0.02M NiL catalyst $(ClO_4)_2$, 4.0ml of 0.14M Malonic acid. Following the addition of these components, integrate 15ml of 3.5M Hydrogen peroxide, ensuring that the total volume of the resultant reaction mixture accumulates to 40ml.

Immediately after preparation of the reaction mixture, the time-dependent potential was recorded. To minimize variation associated with the oscillation phase, an equal volume of each sample solution was systematically introduced at the seventh potential minimum, which was identified experimentally as the most suitable perturbation point.

Results and Discussion

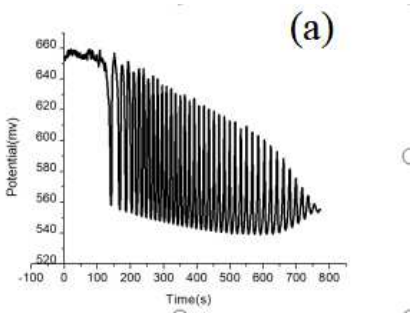
Classic B-R Chemical Oscillator System

Following the experimental procedure described above, a Briggs–Rauscher chemical oscillator

system (H_2SO_4–KIO_3–MA–$[NiL](ClO_4)_2$–H_2O_2) was established. After a brief induction period, regular potential oscillations appeared once the hydrogen peroxide solution had been added and the mixture thoroughly homogenized. The solution simultaneously underwent periodic color changes from light yellow to orange-yellow and then to brown before the sequence repeated. These changes are associated with the redox cycling of nickel species; during the reaction, one-electron transfer occurs between divalent and trivalent nickel. The corresponding potential–time profile is shown in Fig. 1a and displays the characteristic periodic behavior of the established chemical oscillator.

Distinguishing R-BINOL and S-BINOL using the BR System

Under otherwise identical conditions, equal volumes of R-BINOL and S-BINOL solutions at the same concentration were added at the same oscillation minimum; the seventh minimum was experimentally identified as the most reproducible addition point. When 50 μL of 0.001 mol/L R-BINOL or S-BINOL was introduced (final concentration 1.25×10^{-6} mol/L), the B-R oscillator was perturbed and temporarily ceased oscillating. The response, however, differed between the two enantiomers: R-BINOL produced an inhibition time (t_in) of 255.6 s, whereas S-BINOL produced a shorter inhibition time of 183.5 s (Fig. 1b,c). As the concentration increased, the inhibitory effects of 100 μL of 0.001 mol/L solutions (final concentration 2.5×10^{-6} mol/L) of R-BINOL and S-BINOL became more pronounced, with inhibition times of 360.8 s and 348.1 s, respectively. R-BINOL still exhibited a longer inhibition time than S-BINOL (Fig. 1d,e). At a further increased concentration (50 μL of 0.005 mol/L, final concentration 6.25×10^{-6} mol/L), the inhibition times of both enantiomers increased significantly, reaching 1538.4 s for R-BINOL and 1131.6 s for S-BINOL. After addition of R-BINOL at this concentration, the oscillation frequency also decreased markedly following recovery of the system (Fig. 1f,g). Thus, across the examined concentration range, R-BINOL consistently produced a longer inhibition time than S-BINOL, providing a measurable basis for discriminating the two enantiomers.



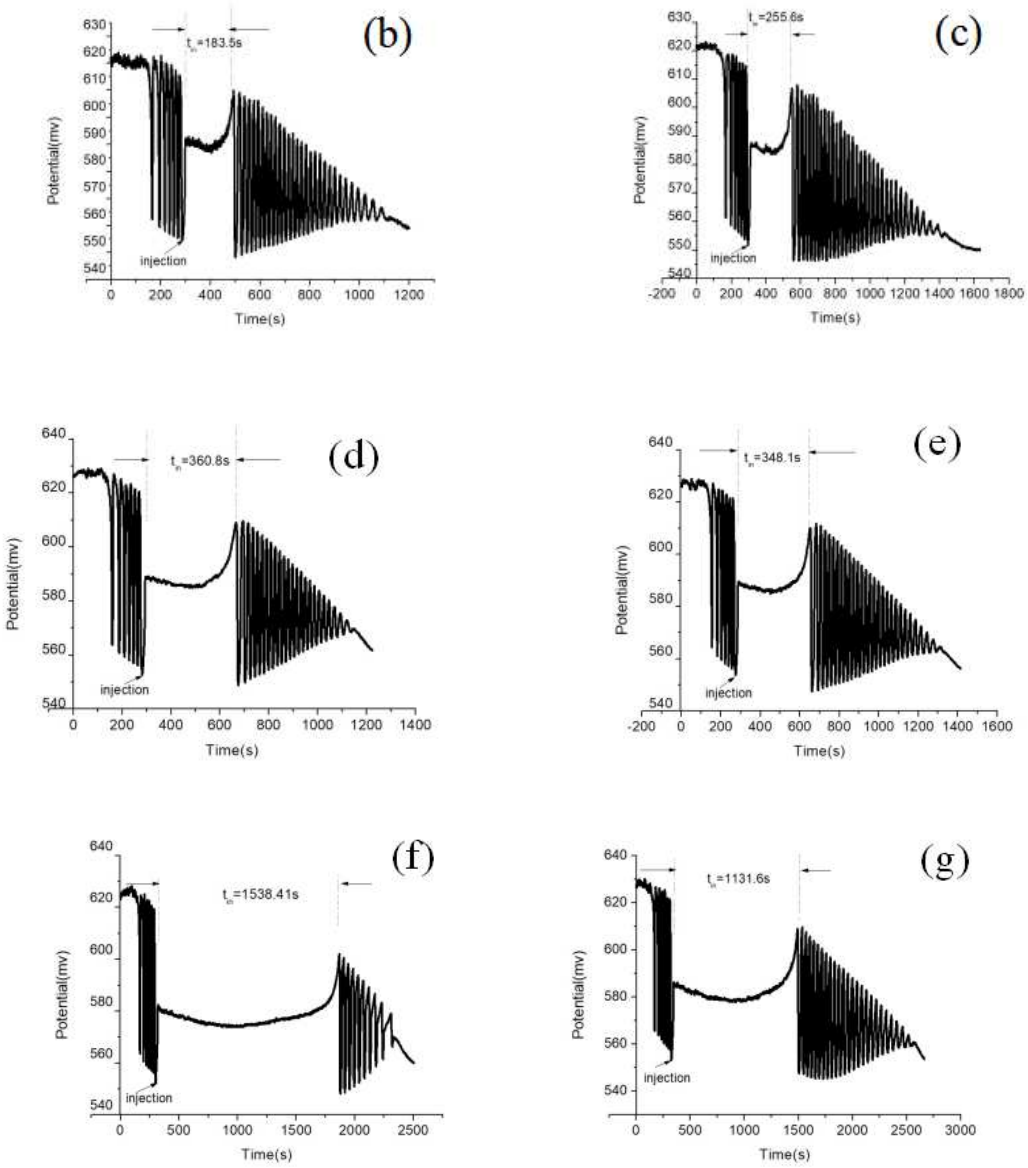


Fig. 1 Oscillation profiles of the Briggs-Rauscher oscillatory chemical system recorded with a platinum working electrode versus a saturated calomel electrode. (a) Unperturbed oscillator after addition of H2O2, showing regular potential oscillations with accompanying color changes. (b) Temporary cessation of oscillations (inhibition time t_in = 255.6 s) following addition of 1.25 × 10^{-6} mol/L R-BINOL at the seventh potential minimum. (c) Temporary cessation (t_in = 183.5 s) following addition of 1.25 × 10^{-6} mol/L S-BINOL under identical conditions. (d) Inhibition (t_in = 360.8 s) by 2.5 × 10^{-6} mol/L R-BINOL. (e) Inhibition (t_in = 348.1 s) by 2.5 × 10^{-6} mol/L S-BINOL. (f) Prolonged inhibition (t_in = 1538.4 s) by 6.25 × 10^{-6} mol/L R-BINOL, with reduced oscillation frequency after recovery. (g) Inhibition (t_in = 1131.6 s) by 6.25 × 10^{-6} mol/L S-BINOL. All sample additions were performed at the seventh potential minimum to ensure phase consistency. Common experimental conditions: [H_2SO_4] = 0.025 mol/L, [KIO_3] = 1.625 × 10^{-2} mol/L, [NiL](ClO_4)$_2$ = 4.375 × 10^{-3} mol/L, [H_2O_2] = 1.5375 mol/L, [MA] = 0.175 mol/L, temperature T = 4 ± 0.5 °C, total volume = 40 mL.

Based on the scatter plots relating the concentrations of R-BINOL and S-BINOL to the inhibition time (t_in), first-order linear correlations were obtained for both enantiomers (Fig. 2). Within the concentration range of 1.25×10^{-6} mol/L to 6.25×10^{-6} mol/L, the correlation coefficient R^2 for R-BINOL is 0.9904, and the linear equation is $t_in = 2.59 \times 10^8 \times C_R\text{-}BINOL - 112.51$. For S-BINOL, $R^2 = 0.9607$ and the corresponding linear equation is $t_in = 2.12 \times 10^8 \times C_S\text{-}BINOL - 110.80$.

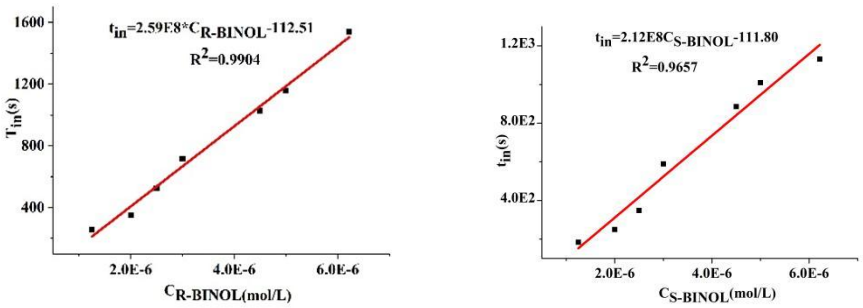


Fig. 2 Linear correlation between the concentration of the added enantiomer and the observed inhibition time (t_in) of the Briggs-Rauscher oscillations. Left panel: R-BINOL, with the linear fit $t_in = 2.59 \times 10^8 \times C_R\text{-}BINOL - 112.51$ ($R^2 = 0.9904$). Right panel: S-BINOL, with the linear fit $t_in = 2.12 \times 10^8 \times C_S\text{-}BINOL - 110.80$ ($R^2 = 0.9607$). Data points correspond to final concentrations in the range 1.25×10^{-6} to 6.25×10^{-6} mol/L. Common experimental conditions: $[H_2SO_4] = 0.025$ mol/L, $[KIO_3] = 1.625 \times 10^{-2}$ mol/L, $[NiL](ClO_4)_2 = 4.375 \times 10^{-3}$ mol/L, $[H_2O_2] = 1.5375$ mol/L, [MA] = 0.175 mol/L, temperature $T = 4 \pm 0.5$ °C.

Exploration of Oscillator System Response Mechanism

Mechanism of Classic Oscillator Systems

The operating principle of this system under flow conditions was initially developed from the NF model investigated by De Kepper, Epstein, and co-workers [22-23] and was subsequently described as the DE (De Kepper-Epstein) model [24]. As experimental evidence accumulated, Furrow et al. extended the earlier mechanistic framework by explicitly incorporating the hydroperoxyl radical as a reaction intermediate. This development led to the widely used Free Radical Controlled Autoinhibition (FCA) model [25], which comprises 12 elementary reaction steps [26] and provides a useful basis for interpreting inhibition in the present B-R system.

$$HOI + I^- + H^+ \leftrightarrow I_2 + H_2O \quad (1)$$

$$HIO_2 + I^- + H^+ \rightarrow 2HOI \quad (2)$$

$$IO_3^- + I^- + 2H^+ \leftrightarrow HIO_2 + HOI \quad (3)$$

$$2HIO_2 \rightarrow IO_3^- + HOI + H^+ \quad (4)$$

$$IO_3^- + HIO_2 + H^+ \leftrightarrow 2IO_2\bullet + H_2O \quad (5)$$

$$2HOO\bullet \rightarrow H_2O_2 + O_2 \quad (6)$$

$$HOI + H_2O_2 \rightarrow I^- + O_2 + H^+ + H_2O \quad (7)$$

$$IO_2\bullet + [NiL]^{2+} + H^+ \leftrightarrow [NiL]^{3+} + HIO_2 \quad (8)$$

$$H_2O_2 + [NiL]^{3+} \rightarrow [NiL]^{2+} + HOO\bullet + H^+ \quad (9)$$

$$HOO\bullet + IO_3^- + H^+ \rightarrow O_2 + H_2O + IO_2\bullet \quad (10)$$

$$MA \leftrightarrow MA(enol) \quad (11)$$

$$I_2 + MA(enol) \rightarrow MAI(IMAI) + H_2O \quad (12)$$

Investigation of Disturbance Mechanism in the System by R-BINOL, S-BINOL

Inspection of the oscillation profiles revealed clear changes after the introduction of R-BINOL or S-BINOL. These changes most likely arise from interactions between the added enantiomer and either the reaction substrates or continuously generated intermediates, followed by oxidation and eventual consumption of the additive.

(1) Cyclic Voltammetry (CV) Experiment

To identify the species responsible for reacting with R-BINOL and S-BINOL, each enantiomer was separately added to acidic solutions containing KIO_3, the catalyst $[NiL]^{2+}$, malonic acid, or hydrogen peroxide, and cyclic voltammetric scans were recorded. No significant influence of either enantiomer was observed on the oxidation peak potentials of $[NiL]^{2+}$ or malonic acid (data not shown). This behavior is consistent with the reducing character of BINOL and malonic acid and with the substantial separation between their reduction-peak potentials, which limits direct electrochemical interference. In the cyclic voltammetry of $[NiL]^{2+}$, the high redox potential between $[NiL]^{2+}$ and $[NiL]^{3+}$ also prevented coupling with the oxidation current of BINOL.

In the KIO_3–H_2SO_4 system, the maximum oxidation peak potential decreased from 1.327 V to 1.242 V upon addition of R-BINOL (Fig. S1, left) and to 1.228 V upon addition of S-BINOL (Fig. S1, right). Both enantiomers thus lowered the KIO_3 oxidation potential to a similar extent (difference of only 14 mV). This observation suggests that the distinct oscillatory responses of R-BINOL and S-BINOL are unlikely to originate from direct interaction with KIO_3.

Relative to the H_2O_2–H_2SO_4 mixture alone, addition of R-BINOL produced a distinct oxidation peak at 0.818 V (Fig. S2, left), indicating that R-BINOL can be oxidized by H_2O_2 or by reactive intermediates generated during the scan. Addition of S-BINOL similarly produced an oxidation peak at 0.859 V (Fig. S2, right). Although both enantiomers altered the voltammetric response in the same general manner, their oxidation-peak potentials differed by 41 mV. The lower peak potential observed for R-BINOL indicates that it is oxidized more readily than S-BINOL under these

conditions.

These voltammetric results provide evidence for redox reactions between R-BINOL or S-BINOL and hydrogen peroxide or its reactive intermediates under the scanning conditions. In the oscillatory experiments, the concentration of each test sample was very low, with the highest final concentration reaching only 6.25×10^{-5} mol/L. By comparison, the concentration of hydrogen peroxide, the substrate of the BR reaction, stood at 1.5375 mol/L, approximately 105 times higher than that of the test samples. Given the extremely low concentration, it was probable that the samples were oxidized as soon as they were added to the BR system, which prevented any inhibitory effect from taking place. However, the CV plots suggested that an intermediate – possibly HOO• – from the BR reaction could have been involved in a redox reaction with the additives. When the CV plots of R-BINOL and S-BINOL in the hydrogen peroxide system were compared, the positions of their secondary oxidation peaks diverged visibly – at 0.818V and 0.859V, respectively. Thus, R-BINOL was more likely than S-BINOL to yield an oxidation current in the hydrogen peroxide system, suggesting that it was more impactful on the chemical oscillation than S-BINOL.

(2) Infrared Analysis of Oxidative Products of R-BINOL and S-BINOL

To determine whether the two hydroxyl groups of R-BINOL and S-BINOL were oxidized, each enantiomer was subjected to the chemical oscillation reaction, and the recovered products were analyzed by infrared spectroscopy. Following the standard experimental procedure, approximately 40 mL of reaction mixture was obtained. Because water in the B-R system can interfere with the infrared region associated with hydroxyl stretching, the products were extracted with dichloromethane. A total of 600 mL of dichloromethane was used over three extraction steps, corresponding to approximately 200 mL per extraction. The combined organic phase was concentrated to 10 mL, dehydrated, and then analyzed.The infrared spectrum (Fig. S3a) demonstrated the stretching vibration peak of -OH in the test substance R-binolphenol (raw material) at 3510 cm^{-1} and a broad absorption peak at 3430 cm^{-1}, corresponding to the hydroxyl peak in water. Compared to the infrared spectrum of R-BINOL, the stretching vibration absorption peaks of C=O in the oxidized products of R-BINOL occur at 1630 cm^{-1} and 1787 cm^{-1}. This indicates oxidation of both hydroxyl groups of R-BINOL in the B-R system. Similarly, Fig S3(b) shows the oxidation of both hydroxyls in S-BINOL.

(3) UV-Visible Analysis of Oxidative Products of R-BINOL and S-BINOL

R-BINOL and S-BINOL were separately added to the chemical oscillation system described above. After the oscillations had ended, the reaction solutions were collected and their UV-visible absorption spectra were monitored over time. For each enantiomer, a final concentration of $6.25*10^{-5}$ M was used, and the oscillation experiment was repeated six times. The extracted products were combined in the same 10 mL volumetric flask for subsequent UV-visible measurements. The product solutions were sealed and stored at 4 °C, and spectra were recorded once daily for six consecutive days. As shown in Figure S4, the maximum absorbance (493 nm^{-1}) decreased with storage time, indicating that the oxidation products were unstable and continued to degrade. The absorbance of the R-BINOL-derived products decreased more rapidly than that of the S-BINOL-derived products. This result is consistent with the cyclic voltammetry data and further supports the conclusion that R-BINOL undergoes oxidation more readily than S-BINOL under the investigated conditions.

On the basis of the proposed reaction mechanism, reactions (13) and (14) consume HOO•

radicals and therefore compete with reaction (10). Depletion of HOO• through these additional pathways disrupts the radical balance required to sustain the oscillatory cycle. According to reactions (8)–(10), the resulting change in HOO• concentration perturbs the coupled interconversion of $[NiL]^{2+}$ and $[NiL]^{3+}$. When this redox cycling is temporarily suppressed, the potential oscillations cease and an inhibition interval is observed. Once the added R-BINOL or S-BINOL has been consumed and the radical balance is restored, the system resumes oscillation. This interpretation links the macroscopic inhibition response to competition for a key radical intermediate in the FCA mechanism.

The difference in inhibition time may be associated with different effective reaction barriers for the oxidation of R-BINOL and S-BINOL by HOO•. Relative to S-BINOL, R-BINOL appears to undergo oxidation more readily and may therefore have a lower effective barrier for reaction with HOO•, resulting in stronger depletion of this radical and a longer inhibitory response. Franz [27] first demonstrated a relationship between HOO• availability and inhibition time by showing that the introduction of a radical inhibitor, superoxide dismutase (SOD), into a B-R oscillatory system caused temporary inhibition. That observation is mechanistically analogous to the inhibition detected here after introduction of the two optical isomers.

Subsequently, R. Cervellati et al [28] confirmed that insufficient HOO• radical availability can produce inhibition in B-R oscillatory chemical systems. Numerous later studies have further examined the relationship between radical-scavenging behavior and inhibition time. In the present system, the combined oscillometric, cyclic-voltammetric, infrared, and UV-visible results consistently support an interpretation in which R-BINOL and S-BINOL interact with HOO• to different extents. Nevertheless, direct identification of all transient intermediates would be required to establish the detailed reaction pathway conclusively. (see scheme 3 in supplementary materials)

Accordingly, the cyclic voltammetry and infrared spectroscopic results provide a basis for proposing the oxidation products and reaction pathways of R-BINOL and S-BINOL in the oscillatory system, as represented in reactions (13) and (14). This proposal is consistent with the observed formation of carbonyl-containing products and the different electrochemical oxidation potentials of the two enantiomers. (Figure S5)

Conclusion

A variety of analytical techniques are available for distinguishing enantiomers; the present study explores a complementary strategy based on chemical oscillations. Both R-BINOL and S-BINOL temporarily inhibited the B-R oscillatory process, but they produced different inhibition times under identical conditions. R-BINOL consistently generated a longer inhibition interval than S-BINOL. Within the concentration range of 1.25×10^{-6} mol/L to 6.25×10^{-6} mol/L, the two enantiomers could therefore be qualitatively discriminated through their distinct effects on the H_2SO_4–KIO_3–MA–H_2O_2–$[NiL](ClO_4)_2$ oscillatory system. Infrared spectroscopy indicated that both enantiomers formed comparable carbonyl-containing oxidation products, whereas cyclic voltammetry and the time-dependent UV–visible spectra showed that R-BINOL was oxidized more readily and that its derived products degraded more rapidly than those of S-BINOL. These observations support the hypothesis that R-BINOL interacts more readily with the HOO• radical intermediate, causing stronger perturbation of the radical balance and a longer inhibition time. The proposed method offers a simple electrochemical approach to chiral discrimination and may inform the development of additional enantiomer-selective assays based on nonlinear chemical dynamics. More broadly, the

findings contribute to understanding the complex reaction mechanisms that underlie dissipative structures such as chemical oscillators.

Author Contributions Statement

Lanlan Zhang: Conceptualization, Methodology, Investigation, Writing – Original Draft, Visualization. Ali Tao: Validation, Formal analysis, Investigation, Data Curation. Ling Zhu: Resources, Software, Investigation. Gang Hu: Conceptualization, Supervision, Project administration, Funding acquisition, Writing – Review & Editing.

Acknowledgment

The authors gratefully acknowledge funding for this work from Natural Science Research Foundation of the Department of Education of Anhui Province(2023AH051808). Teaching Innovation Team for Basic Chemistry Course Group(2025cxtd085). Scientific Research Project of Anhui Provincial Department of Education: Study on Construction of Fingerprints of Volatile Components of Dendrobium huoshanense Based on GC-IMS (No. 2024AH050620).

Declaration Statement

Declaration of Competing Interest

The authors declare that they have no known competing financial interests or personal relationships that could have appeared to influence the work reported in this paper.

Data Availability Statement

The data that support the findings of this study are available from the corresponding author upon reasonable request.

Ethics Statement

This study does not involve human subjects or animal experiments, and therefore no ethical approval was required.

References

1. Tang W, Zhang X (2003) New chiral phosphorus ligands for enantioselective hydrogenation. Chem Rev 103:3029 – 3070

2. Kolb HC, VanNieuwenhze MS, Sharpless KB (1994) Catalytic asymmetric dihydroxylation. Chem Rev 94:2483–2547

3. Zhang Jin, Zhang Lingjun, Peng Tianying, et al (2018) Synthesis of (S)-6-vinyl-2,2′-methylenedioxy-1,1′-binaphthalene. Journal of Hunan City University (Natural Science Edition) 91:78–81

4. Jiang Shengqian, Wang Zhouyu, Jiang Zhenju, et al (2011) Synthesis of (R)-3,3′-dicarbo xylic acid-1,1′-binaphthol. Journal of Xihua University (Natural Science Edition) 30:99–101

5. Huang Y (2002) Synthesis and resolution of naphthylamine (NOBIN) [Dissertation]. Sichuan Normal University

6. Liu W (2012) Synthesis and performance study of chiral fluorescent dyes based on binaphthol [Dissertation]
7. Polavarapu PL (1998) Chiroptical Spectroscopy: Fundamentals and Applications. Appl Spectrosc 52:1319–1330
8. Li Qianqian, Jia Hongzhi, Wang Kai (2008) Research and Implementation of a New Measurement Method for Laser Polarimeter. Optical Instrument 29:61–64
9. Reinscheid UM (2010) Content-based structure comparison and analysis of chiral molecules in two and three dimensions. J Cheminform 2:1–24
10. Andersson T, Borhan B, Berova N (2000) Absolute configurational assignment of 3-hydroxycarotenoids. J Chem Soc Perkin Trans 1:256–269
11. Dale JA, Mosher HS (1973) Nuclear magnetic resonance enantiomer reagents. Configurational correlations via nuclear magnetic resonance chemical shifts of diastereomeric mandelate, O-methylmandelate, and α-methoxy-α-trifluoromethylphenylacetate (MTPA) esters. J Am Chem Soc 95:512–519
12. Joshi BS, Pelletier SW (1999) A cautionary note on the use of commercial (R)-MTPA-Cl and (S)-MTPA-Cl in determination of absolute configuration by Mosher ester analysis. Heterocycles 51:183–184
13. Zielinski P, Cyrański MK, Leśniewska B, Umecki P, Wójcik KW (2012) Stereochemistry of 1,1′-Bi-2-naphthol Revisited. Molecules 17:10670–10678
14. Harada N (2008) Determination of absolute configurations by X-ray crystallography and 1H NMR anisotropy. Chirality 20:691–723
15. Bijvoet JM, Peerdeman AF, Van Bommel AJ (1951) Determination of the absolute configuration of optically active compounds by means of X-rays. Nature 168:271–272
16. Ma Shuguo, Wu Guozhen (1998) Review of Raman Optical Activity Research on Chiral Substances. Journal of Light Scattering 13:94–270
17. Wang Juan, Yang Xiaodi (2012) Spectral Identification of Absolute Configuration of Chiral Compounds – From Instrumental Characterization to Theoretical Calculation. College Chemistry 12:23–25
18. Feng ZC, Li C (2015) The new progress of Raman optical active spectroscopy in chirality research. In: Proc 18th Natl Conf Light Scatt
19. Sánchez-Hernández L, Castro-Puyana M, Lucio-Cazaña FJ, Marina ML (2013) Chiral ligand-exchange capillary electrophoresis and high-performance liquid chromatography using amino acids and dipeptides as chiral selectors. Electrophoresis 34:1270–1279
20. Ciogli A, Ismail OH, Mazzoccanti G, et al (2018) Enantioselective ultra high performance liquid and supercritical fluid chromatography: The race to the shortest chromatogram. J Sep Sci 41:224–227
21. Curtis NF (1974) Some metal-ion complexes with ligands formed by reaction of amines with aliphatic carbonyl compounds. Part I. Nickel(II) and copper(II) complexes formed by the diaminoethane-acetone reaction. J Chem Soc Dalton Trans:1357–1361
22. Noyes RM, Furrow SD (1982) The oscillatory Briggs-Rauscher reaction. A skeleton mechanism for oscillations. J Am Chem Soc 104:45–48
23. De Kepper P, Epstein IR, Kustin K, Orban M (1982) Systematic design of chemical oscillators. Part 8. Batch oscillations and spatial wave patterns in chlorite oscillating systems. J Phys Chem 86:170–171

24. Furrow SD, Cervellati R, Amadori G (2002) New substrates for the oscillating Briggs-Rauscher reaction. J Phys Chem A 106:5841–5850. https://doi.org/10.1021/jp0138779
25. Uddin W, Hu G, Hu L, Hu YY, Fang ZH, Rooh U, Sun XX, Zhang Y, Song JM (2017) Identification of two aromatic isomers between 2- and 3-hydroxy benzoic acid by using a Briggs-Rauscher oscillator. J Electroanal Chem 803:135–140
26. Ivanov VL, Lyashkevich SY (2016) Peculiarities in the photochemical behavior of 1-bromo-2-hydroxynaphthalene in cetylpyridinium chloride micellar solution. High Energy Chem 50:32–36
27. Franz DA (1991) Superoxide dismutase and the Briggs-Rauscher reaction. J Chem Educ 68:57
28. Cervellati R, Höner K, Furrow SD, Neddens C, Costa S (2001) The Briggs-Rauscher reaction as a test to measure the activity of antioxidants. Helv Chim Acta 84:3533–3547

Supplementary materials

Scheme 1. Chemical structures of R-1,1′-bi-2-naphthol (R-BINOL, left) and S-1,1′-bi-2-naphthol (S-BINOL, right).
Scheme 2. Structure of the ligand L·2$HClO_4$ (left) and the macrocyclic nickel catalyst [NiL]$(ClO_4)_2$ (right), where L = 5,7,7,12,14,14-hexamethyl-1,4,8,11-tetraazacyclotetradeca-4,11-diene.
Scheme 3. Proposed oxidation of R-BINOL or S-BINOL by hydroperoxyl radicals (HOO•) to yield the same product, (Z)-2H,2′H-[1,1′-binaphthalenylidene]-2,2′-dione.

Figure S1. Cyclic voltammograms of the KIO_3–H_2SO_4 mixed solution (black) and the same solution containing a low concentration of R-BINOL (red, left panel) or S-BINOL (red, right panel). Conditions: [H_2SO_4] = 0.025 mol/L, [KIO_3] = 1.625×10^{-2} mol/L, [R-BINOL] or [S-BINOL] = 6.25×10^{-6} mol/L, scan rate = 100 mV/s.
[H_2SO_4]= 0.025 mol/L, [KIO_3]= 1.625×10^{-2} mol/L, [R-BINOL]= 6.25×10^{-6} mol/L, [S- BINOL]= 6.25×10^{-6} mol / L, scanning rate=100mv/s
Figure S2. Cyclic voltammograms of the H_2O_2–H_2SO_4 mixed solution (black) and the same solution containing a low concentration of R-BINOL (red, left panel) or S-BINOL (red, right panel). Conditions: [H_2SO_4] = 0.025 mol/L, [H_2O_2] = 1.5375 mol/L, [R-BINOL] or [S-BINOL] = 6.25×10^{-6} mol/L, scan rate = 100 mV/s.
[H_2SO_4]= 0.025 mol/L, [H_2O_2]= 1.5375 mol/L， [R-BINOL]= 6.25×10^{-6} mol/L, [S- BINOL]= 6.25×10^{-6} mol / L, scanning rate=100mv/s
Figure S3. Infrared spectra of (a) R-BINOL (starting material) and its oxidation products recovered after the Briggs–Rauscher reaction; (b) S-BINOL (starting material) and its oxidation products. The appearance of C=O stretching bands indicates conversion of the hydroxyl groups.
Figure S4. Time-dependent UV–Vis spectra of the oxidation products of (a) R-BINOL and (b) S-BINOL recovered after the oscillatory reaction (final concentration of each enantiomer = 6.25×10^{-5} mol/L). Spectra were recorded daily for six consecutive days after storage at 4 °C. The absorbance maximum at approximately 493 nm decreases with time, indicating progressive degradation of the oxidation products.
Figure S5. Schematic reaction coordinate diagram for the oxidation of R-BINOL and S-BINOL by HOO• radicals. The diagram illustrates that R-BINOL has a lower activation energy barrier in the intermediate state relative to S-BINOL, consistent with its stronger inhibitory effect.

Supplementary Files

This is a list of supplementary files associated with this preprint. Click to download.

- Supplementarymaterials.docx